

International Conference on Space Optics—ICSO 2006

Noordwijk, Netherlands

27–30 June 2006

Edited by Errico Armandillo, Josiane Costeraste, and Nikos Karafolas



Radiation hardness assessment of widely tunable and DFB lasers

Michael Todd, Tom Farrell,



RADIATION HARDNESS ASSESSMENT OF WIDELY TUNABLE AND DFB LASERS

Michael Todd, Tom Farrell

*Intune Technologies, 9c Beckett Way, Parkwest Business Park, Dublin 12, Ireland.
Email: michael.todd@intunetech.com*

ABSTRACT

Proton irradiation was carried out on emerging semiconductor laser technologies, including Distributed Bragg Reflector (DBR) and Sampled Grating (SG)-DBR lasers at 1550 nm, as well as Distributed Feedback (DFB) lasers at 935 nm and 1550 nm. Two separate exposure sessions, at low and high doses, were performed, the first to mimic a typical 2-year Earth Observation mission, and the second for more comprehensive radiation hardness assessment. Low dose exposure yielded minimal damage to all lasers, but the 935 nm DFBs did exhibit small changes in tuning efficiency. In-situ measurements on the 1550 nm DFB and DBR lasers show degradation in lasing threshold by 15% and 4% respectively, and the DBR mode structure is maintained but shifts by more than one mode width.

1. INTRODUCTION

Radiation testing of semiconductor lasers has been limited to single-frequency devices, such as Fabry-Perot, Distributed Feedback (DFB) and Vertical Cavity Surface Emitting lasers. These are the most common lasers in the communications industry, and are the first to be deployed in space missions. This report presents results of radiation testing of emerging semiconductor laser technologies, including Distributed Bragg Reflector (DBR) and Sampled-Grating (SG) DBR lasers. These lasers are widely tunable between 1525 – 1565 nm and not only hold promise to replace existing laser technology in telecommunications, but also have useful applications in sensing and monitoring. No tests on radiation hardness have been done previously on these new devices. In addition to the widely tunable lasers, new DFB lasers at 935 nm, as well as a DFB at 1550 nm have been tested.

Of the damage mechanisms caused by radiation displacement damage is the main source of degradation in semiconductor lasers. On a microscopic level, semiconductor lasers consist of a highly ordered lattice of atoms. The displacement energy of an atom typically ranges from 25 – 100 eV depending on the crystal material and structure. Electron and proton interactions that transfer 25 – 1000 eV of energy to an atom produce a defect (vacancy-interstitial pair, or Frenkel defect) by displacing the atom from its lattice site. At room temperature, ninety percent of these defects recombine resulting in no net damage. At higher particle energies and fluence however, a cascading effect can cause an

extended region of defects. For particle energies above 10 keV, extended defects become problematic. The semiconductor parameter most sensitive to lattice damage is carrier lifetime, which will affect lasing threshold. Additionally, lattice damage cause carrier removal, changing doping concentration and leading to a loss in output power. Further, internal absorption can increase, although the short cavities in modern laser design minimise this effect.[1]

Annealing from current injection results in the recombination of Frenkel defects, which can lead to an underestimate of radiation damage. Not all work has taken annealing into account, making it hard to compare results between tests. Injection annealing is a crucial issue that needs to be considered when investigating actual damage due to radiation. To reduce the degree of annealing, the diagnostic tests of the lasers have been performed under sessions of <1 minute, and where possible, the injection current was pulsed with 22 μ s width, 12% duty cycle.

2. EXPERIMENT

Two irradiation sessions were carried out at the Paul Scherrer Institut (PSI), one using 10 MeV protons at low flux and low fluence, and the second with 50 MeV protons at high flux and fluence. Low fluence irradiation of $4 \times 10^9 \text{ cm}^2$ was designed to mimic the exposure expected in a typical 2-year Earth Observation (EO) mission, with 4 mm spherical aluminium shielding and a factor of two in design margin. Total dose was calculated using ESA's Space Environment Information System (SPENVIS). High-flux, high-energy irradiation was used for a more complete radiation hardness assessment of the lasers. For these tests, the lasers were exposed to 50 MeV protons and a fluence of $1.8 \times 10^{13} \text{ cm}^{-2}$.

Two sets of lasers were exposed, each set containing the five types of lasers listed in Table 1. The proton beam profile at PSI was approximately 10 cm in diameter and the central region within ~3 cm radius provided <10% variation in proton flux. Therefore the lasers were mounted onto a breadboard within a <6 cm diameter footprint. The 935 nm DFB lasers and SG-DBR were grounded during exposure, while the Avanex DFB and JDSU DBR lasers were monitored in real-time using pulsed current sources and short measurement times.

Table 1 List of the types of lasers that were tested. Separate sets of lasers were used for low- and high-energy exposure.

Laser	Manufacturer	Wavelength	Package
DFB	FBH	935 nm	TO9 w/o TEC
DFB	Nanoplus	935 nm	TO8 w/ TEC
DFB	Avanex	1550 nm	14-pin butterfly
DBR	JDSU	1550 nm	14-pin butterfly
SG-DBR	Agility	1550 nm	14-pin butterfly

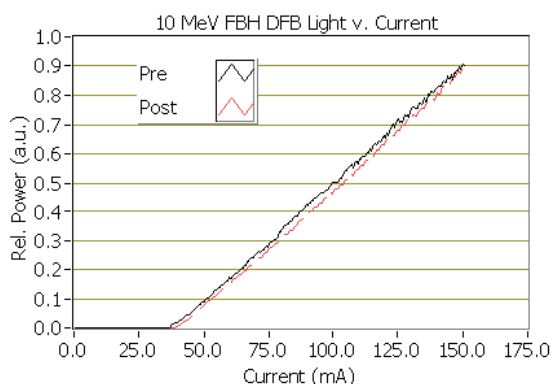


Fig. 1 FBH DFB LIs pre- and post-irradiation.

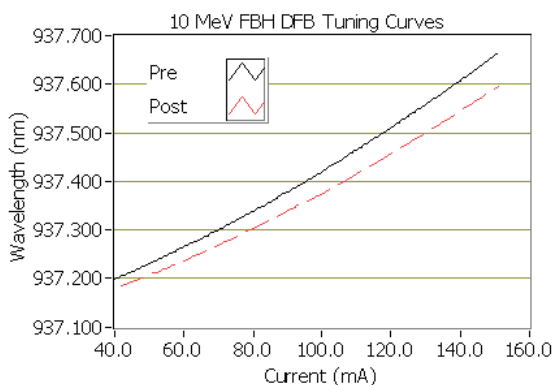


Fig. 2 Tuning curves of the FBH DFB laser before and after 10 MeV proton irradiation.

3. RESULTS

3.1 10 MeV Tests

The overall effects from low dose exposure are minimal. The butterfly packaging of the 1550 nm devices provided shielding which the 935 nm DFB lasers (TO cans with front-end irradiation) did not have. As such, some radiation-induced damage to the latter devices was observed while negligible damage was seen in the butterfly devices.

3.1.1 FBH DFB

Pre- and post-radiation LIs and wavelength tuning curves are shown in Fig. 1 and Fig. 2. Lasing threshold increases slightly from 37 mA to 40 mA and although the slope efficiency is nearly the same, there is a slight change in curvature. The shift in the tuning curves to shorter wavelength as well as a reduced slope of the curve could reflect the small change in slope efficiency.

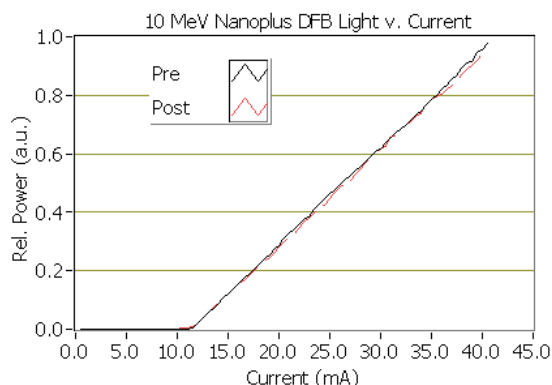


Fig. 3 Nanoplus DFB LIs pre- and post-irradiation.

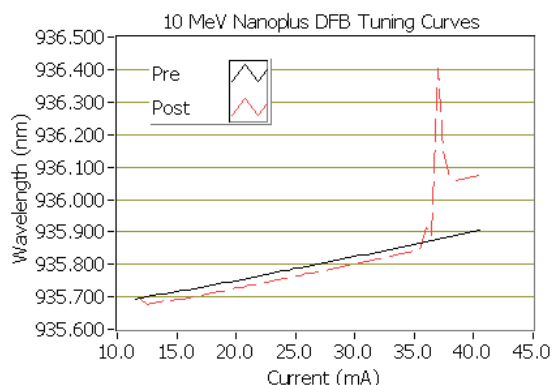


Fig. 4 Tuning curves of Nanoplus DFB at 37 °C.

3.1.2 Nanoplus DFB

Results for the Nanoplus DFB are shown in Fig. 3 and Fig. 4. In this case, the LIs show no degradation in lasing threshold or slope efficiency. The tuning curves show interesting effects: similarly to the FBH device, the wavelength shifts to shorter wavelength and the tuning curves have the same slope. More troubling is the apparent mode hop that occurs at approximately 37 mA, at which point the wavelength jumps ~200 pm. This effect is not due to feedback into the laser from fibre-coupling optics during evaluation. With different coupling configurations as well as deliberately misaligned optics (to reduce potential feedback), the modehop occurs at the same injection current, implying that the observed effect arises internally. One possible cause is increased back reflection from the output

window into the laser. A second option is that a spatial defect in the diode facet could contribute to spurious reflection. In any case, the damage leads to unpredictable behaviour in the laser at highest injection current.

3.1.3 Avanex DFB

In-situ measurements were taken with the Avanex DFB laser. Fig. 5 shows the percent change in lasing threshold over the course of irradiation. The lasing threshold (14 mA) does not change by more than 2%. The lasing threshold measured at Intune in post-radiation testing was also 14 mA. Wavelength measurements (Fig. 6) show <2 pm variation, which is within the resolution of the wavemeter. The jump in wavelength from 1532.432 nm to 1532.437 nm corresponds to the period of time when irradiation was paused in order to increase the flux to a more stable level. During this time, it is possible that the temperature of the laser changed slightly. Subsequent wavelength measurements after the pause show stable laser operation.

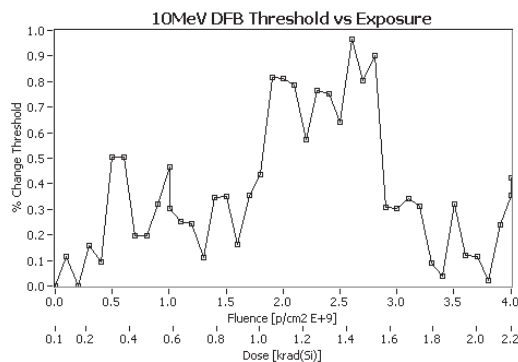


Fig. 5 Change in Avanex DFB lasing threshold during 10 MeV proton exposure

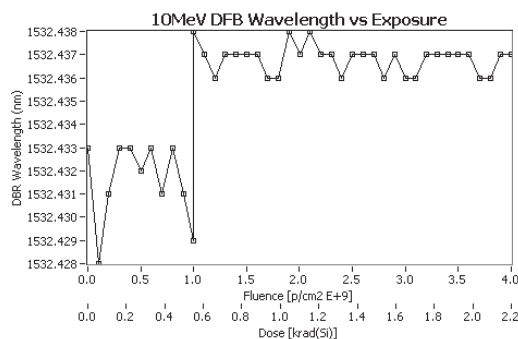


Fig. 6 In-situ wavelength measurement of Avanex DFB laser during irradiation with 10 MeV protons.

3.1.4 JDSU DBR

Lasing threshold of the JDSU DBR laser was also measured in-situ, and the results are shown in Fig. 7.

LIs were obtained by ramping the gain section only, keeping both the Bragg and Phase sections grounded. There is no change in lasing threshold over the course of proton exposure, with variation less than 0.5%. This laser is also packaged in a butterfly housing and therefore it benefits from additional shielding.

Rather than measure wavelength at a particular operating point of the DBR, a more meaningful measurement carried out in-situ along with lasing threshold was a power plane to show any changes in the mode structure. A representative plane is shown in Fig. 8, which was obtained by measuring the received power as a function of Phase and Bragg current. The lasing modes are observed as vertical stripes in the graph and correspond to stable operation. The boundaries between the modes are modehops. Power planes were measured over the course of the irradiation session and the position of mode boundaries was monitored. No observable change in mode position was seen indicating that the laser experienced no damage from the proton exposure.

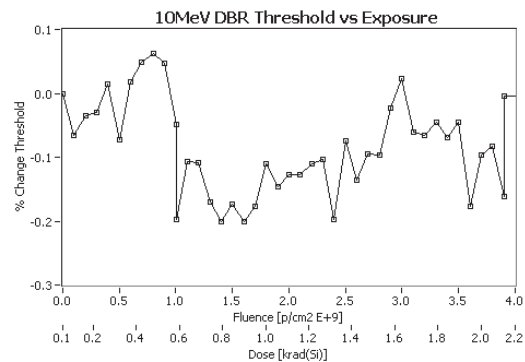


Fig. 7 Measured change in threshold current of JDSU DBR laser during 10 MeV irradiation

3.1.5 Agility SG-DBR

Examples of power planes of the SG-DBR laser are shown in Fig. 9, which reveal its complicated mode pattern. With four active sections in the laser (Front, Gain, Phase, Back) as well as a SOA at the output, many variables control the laser operation. This laser in particular shows some unusual non-linearities in some of the operation cells, however mode boundaries are clear enough to show any changes in laser performance. In these planes, the current in the front and back sections of the laser are ramped in a quadratic fashion. This is because the change in index with injection current ($\partial n/\partial i$) for each section saturates with increasing current, which implies that at higher injection current, a larger change in current is needed to effect the same change in index. Ramping the currents quadratically offsets some of the saturation effects and yields a more linearised mode plane.

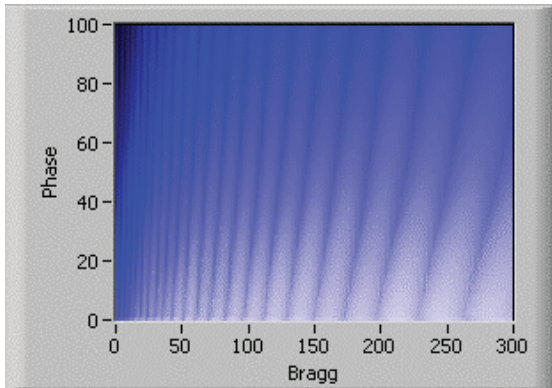


Fig. 8 Example of a measured power plane (Bragg vs. phase) of the JDSU DBR laser measured during proton exposure.

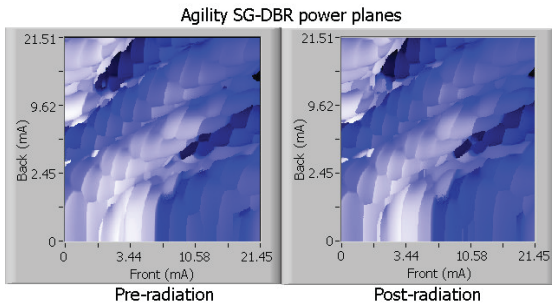


Fig. 9 Power planes scanning Front and Back sections, with Gain/Phase/SOA = 144.9/4.6/100 mA.

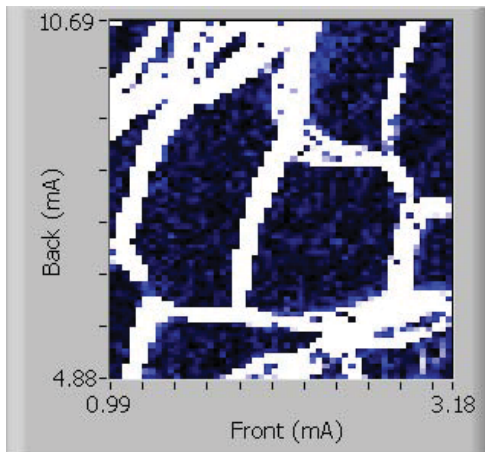


Fig. 10 Close-up region of the Laplace-transformed plane, showing the movement of the mode boundaries.

There is little shift in the mode pattern of the SG-DBR when comparing the planes taken before and after exposure. By subtracting the two planes and applying a 3x3 Laplace operator the mode boundaries become evident. A portion of the-transformed plane is shown in Fig. 10. Here, the white area shows the movement of the mode boundaries between pre- and post- irradiation.

Comparing the width of the boundary region in Fig. 10 to the size of the operating modes, one can conclude that the mode pattern in the laser has changed by 5-10% due to proton irradiation.

Differences in the LIs in pre- and post- radiation can point to shifts in the mode pattern but has limited information in terms of degradation in lasing threshold and efficiency because of the sensitivity of the curves to the mode positions. Fig. 11 shows LI curves when the Gain section was ramped from 0 – 100 mA, for two laser settings. In the first, the Phase, Front, Back and SOA sections (in shorthand referred to as P/F/B/S) are set to P/F/B/S = 0/0/0/100 mA, while in the second, P/F/B/S = 5/10/20/100 mA. The measured LIs before and after proton exposure are compared in each case. In the first case, the pre-radiation curve shows a very soft turn-on to lasing and there are clear mode hops as gain current is increased. After radiation, lasing threshold is unchanged, but the increase in power is continuous. When P/F/B/S = 5/10/20/100 mA in the second graph, there is a very large increase in lasing threshold after radiation exposure, and there are also marked differences in (non-linear) slope efficiency.

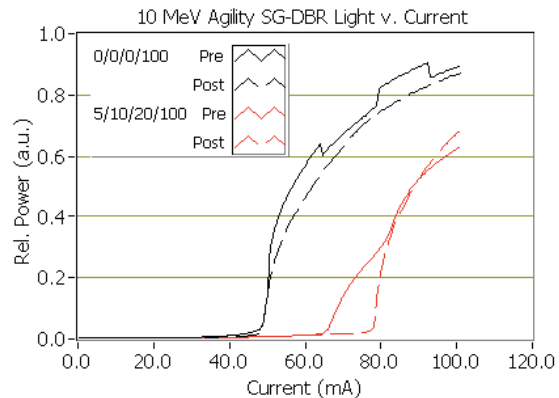


Fig. 11 Pre- and post-irradiation LIs of Agility SG-DBR, ramping Gain with Phase/Front/Back/SOA at two settings, 1) 0/0/0/100 mA and 2) 5/10/20/100 mA.

Lasing threshold is obtained from the first set of LIs with P/F/B/S = 0/0/0/100 mA. The lasing threshold was measured to be 50.0 mA both before and after irradiation. Caution must be taken with this value because lasing threshold can change dramatically with only small changes in mode position, as illustrated in the second graph in Fig. 11. Here, the lasing threshold increases by 18% from 67 mA to 79 mA. Taken at face value, this change in threshold would suggest severe displacement damage in the laser. In actual fact, the shift is due to the sensitivity of lasing threshold to the position of the operating modes in the laser. Akin to the other butterfly-packaged lasers, one should not expect to see significant changes in the SG-DBR at these low

dose levels. Because there is no dramatic change in the mode map, one can conclude that the SG-DBR suffered little radiation damage.

3.2 50 MeV Tests

The set of five lasers that were exposed to high flux 50 MeV protons are still too active for safe handling and are therefore still at PSI. At this time, only in-situ measurements are available on the Avanex DFB and JDSU DBR.

3.2.1 Avanex DFB

The results from high-energy exposure show a significant degradation in laser performance. Measured LIs are shown in Fig. 12 over the course of exposure, in fluence increments of $3.6 \times 10^{12} \text{ cm}^{-2}$. Fig. 13 summarises the change in lasing threshold with increasing fluence. Lasing threshold increases linearly with fluence, by up to 15 %, and the slope efficiency does degrade, but only a very small amount. The results are consistent with other tests on DFBs in the literature and can be attributed to the reduced carrier lifetime caused by displacement damage.

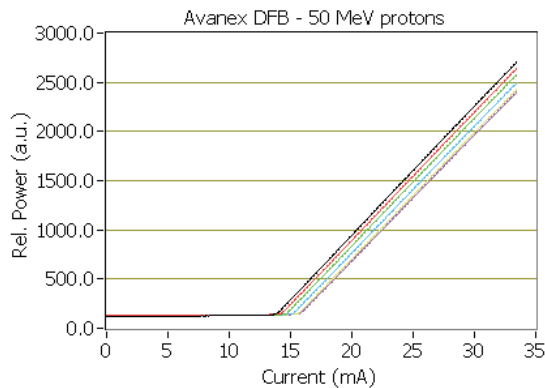


Fig. 12 LIs of Avanex DFB during radiation exposure at fluence = 0 – $1.8 \times 10^{13} \text{ cm}^{-2}$ in increments of $3.6 \times 10^{12} \text{ cm}^{-2}$.

Wavelength stability also degrades, as seen in Fig. 14. Initially, lasing wavelength is stable <2 pm. After approximately 1.5 hours (fluence $\sim 5.4 \times 10^{12} \text{ cm}^{-2}$), the wavelength becomes unstable and tends towards longer wavelength. The uncertainty in the wavelength increases from 2 pm to 10 pm. A shift in wavelength in one direction would be consistent with an associated increase in lasing threshold, but the increased noise in wavelength stability cannot be explained by threshold changes. A possible explanation for the increased instability is that the temperature stability in the laser degraded. In the setup, a fan was placed next to the lasers to remove excess heat from the TEC heatsink. After the irradiation session, it was discovered that the fan had failed, but it is not clear at which point it

stopped working. A plausible explanation may be that it failed after about 1.5 hours, coinciding with the onset of wavelength instability.

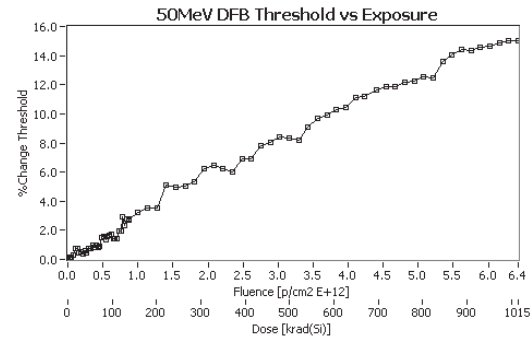


Fig. 13 In-situ change in lasing threshold of Avanex DFB exposed to 50 MeV protons.

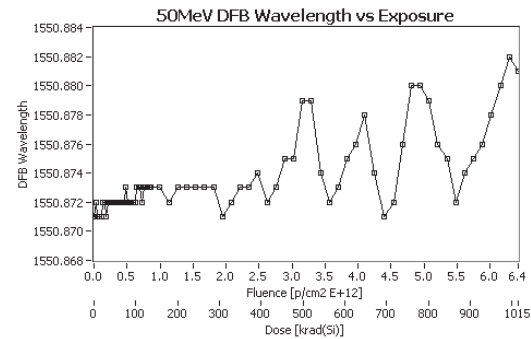


Fig. 14 In-situ measurement of Avanex DFB wavelength during 50 MeV exposure.

3.2.2 JDSU DBR

The lasing threshold in the DBR laser also increased steadily with increasing proton exposure. The percent change in threshold as a function of exposure is shown in Fig. 15. A total of 4% deviation was measured. The mode position also showed an impressive shift. Planes similar to the one shown in Fig. 8 were measured and the mode positions along the Bragg axis at Phase = 0 mA were located over the course of exposure and are shown in Fig. 16. Over the course of the exposure, the mode positions shift to higher current (consistent with an increasing laser threshold) by up to one mode width. Aside from shift, the mode pattern remained intact, which suggests that displacement damage mainly targets laser efficiency but that the spatial defects do not impair the overall characteristics (i.e. tunability) of the laser. Nonetheless, because of the large shift in mode position, if the laser were operated at a specific operating point without active locking, at some point a mode boundary would cross the operating point and result in mode failure. With further proton exposure, the mode boundary would move through the operating point and the laser would operate in single mode again, however at a different, unknown wavelength. Provided the

position of the operating point in the lasing mode is tracked, however, continuous operation of the laser is be possible, even under high proton doses.

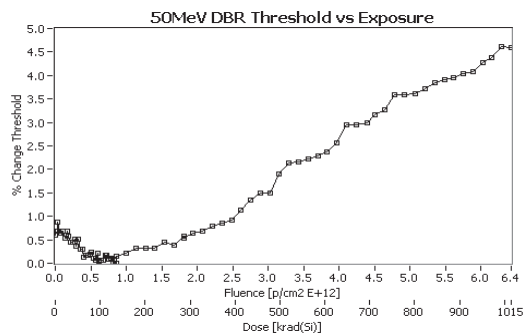


Fig. 15 Change in lasing threshold of JDSU DBR laser measured during 50 MeV proton irradiation.

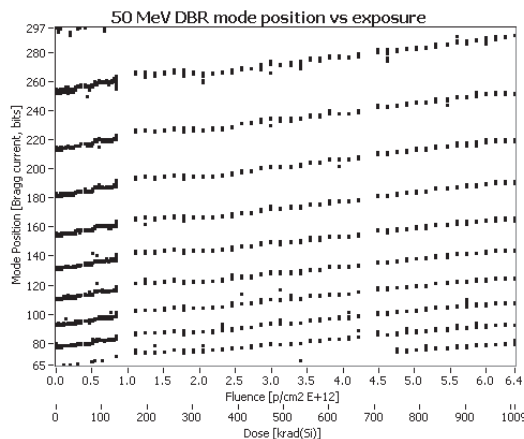


Fig. 16 In-situ change in mode position of the JDSU DBR laser exposed to 50 MeV protons.

4. ASSESSMENT AND CONCLUSIONS

This report investigated proton damage in several types of lasers under both high and low energy exposure. The parameters that are most affected by radiation damage are threshold current and slope efficiency. Low energy exposure, which mimics a typical EO mission, show no significant damage to the laser diodes, although the 935nm devices display higher sensitivity which is likely due to the unshielded TO packaging. However, the change in slope efficiency in the FBH DFB, and the onset of a mode-hop in the Nanoplus DFB tuning are both unexpected at such low doses. Tests on similar InGaAs lasers at 905 nm do not show such a marked degradation in slope efficiency yet do show some unusual features.[2] A strained quantum well laser was exposed to 50 MeV protons and fluence up to $3 \times 10^{13} \text{ cm}^{-2}$. It was found that, compared with the other types of lasers investigated, a relatively large number of bulk defects were present after irradiation.

Similarly, the 935 nm devices tested here may be particularly susceptible to bulk defects, which would adversely affect their performance. Further evaluation will be necessary, particularly with comparison to the devices exposed to high energy.

The 1550 nm DFB exposed to 50 MeV protons show standard degradation from proton irradiation. Displacement damage causes carrier lifetime associated with non-radiative recombination to decrease towards that of spontaneous recombination. The competition between the two mechanisms results in an increase in lasing threshold. Above lasing threshold, however, stimulated recombination lifetime is much shorter than either the spontaneous or non-radiative lifetimes, and so radiation damage has less of an effect on the slope efficiency (typically up to fluence $\sim 10^{14-15} \text{ cm}^{-2}$).[3]

From the current data on widely tunable lasers (DBR and SG-DBR), it appears that displacement damage targets the same parameters as with other semiconductor lasers (i.e. carrier lifetime), affecting the lasing threshold and efficiency. These changes have subsequent effects on laser performance such as mode pattern, but the overall operation of the lasers does not change. Despite the increased complexity of these multi-section lasers, their modal patterns are not adversely influenced by local defects.

1. Johnston, A.H., Radiation effects in light-emitting and laser diodes, *IEEE Trans. Nucl. Sci.*, Vol: 50, 689–703, 2003.
2. Johnston, A.H., Miyahira, T.F. and Rax, B.G., Proton damage in advanced laser diodes, *IEEE Trans. Nucl. Sci.*, Vol 48, 1764-1772, 2001.
3. Gill, K. et al., Comparative Study of Radiation Hardness of Optoelectronic Components for the CMS Tracker Optical Links, Presented at RADECS conference, Oxford, Sept. 1998.